IEEE Photonics Journal
An IEEE Photonics Society Publication

Open Access

Generation of Orbital Angular Momentum Beam With Circular Polarization Ceramic Antenna Array

Volume 11, Number 2, April 2019

Ke Bi
Jianchun Xu
Daquan Yang
Yanan Hao
Xinlu Gao
Shanguo Huang

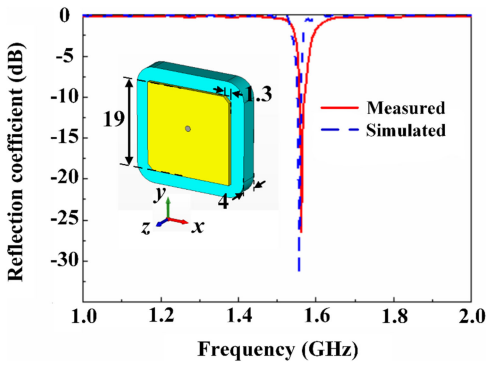

DOI: 10.1109/JPHOT.2019.2899236
1943-0655 © 2019 IEEE

Generation of Orbital Angular Momentum Beam With Circular Polarization Ceramic Antenna Array

Ke Bi,[1,2] **Jianchun Xu**,[1,2] **Daquan Yang**,[1,3] **Yanan Hao**,[1,2] **Xinlu Gao**,[1,2] **and Shanguo Huang** [1,2]

[1]State Key Laboratory of information Photonics and Optical Communications, Beijing University of Posts and Telecommunications, Beijing 100876, China
[2]School of Science, Beijing University of Posts and Telecommunications, Beijing 100876, China
[3]School of Information and Communication Engineering, Beijing University of Posts and Telecommunications, Beijing 100876, China

DOI:10.1109/JPHOT.2019.2899236

Manuscript received January 15, 2019; revised February 2, 2019; accepted February 7, 2019. Date of publication February 13, 2019; date of current version March 1, 2019. This work was supported in part by the National Natural Science Foundation of China under Grant 61774020, Grant 51802023, Grant 61690195, Grant 61605015, and Grant 61575028, in part by the Science and Technology Plan of Shenzhen City under Grant 201887776, in part by the Fund of IPOC BUPT under Grant IPOC2017ZT06, and in part by the Fundamental Research Funds for the Central Universities under Grant 2018XKJC05, China. Corresponding authors: Daquan Yang and Shanguo Huang (e-mail: ydq@bupt.edu.cn; shghuang@bupt.edu.cn).

Abstract: Orbital angular momentum (OAM) beams can be generated at many microwave frequencies by using antenna array. However, the complexity of the system and inability to transmit over long distances limit the applications of OAM beams in the radio domain. Here, a significantly simplified global positioning system (GPS) ceramic antenna array is employed to generate OAM beams without the assistance of phase shifting devices. Simulation of the GPS ceramic antenna array verifies that the OAM beams with the mode of ± 1 show small divergence angle and very standard spiral phase distribution. To test the transmission capability of the proposed antenna array, a measurement system that can detect the one-dimension spatial distribution of electromagnetic characteristic for the OAM beams is set up. Even considering the enormous loss in cables and power divider, the receiving antenna still can receive the electromagnetic characteristic of the OAM beams at a place more than 2 m away from the antenna array. Experimental results presented in this paper demonstrate the excellent performance of the OAM beams when generated with the proposed ceramic antenna array configuration.

Index Terms: Ceramic antenna array, circular polarization, orbital angular momentum beam.

1. Introduction

The total angular momentum contains spin angular momentum and orbital angular momentum (OAM) [1]. The optical OAM beams have been attracting extensive attention owing to their special spatial profile of intensity and phase [2]–[4]. Especially in trapping particles [5], optical imaging [6], [7], rotating microscopic particles [8] and other fields [9]–[11], OAM beams exhibit their distinctive advantages. The OAM beams with different propagating modes are mutually orthogonal with each other [12], which offers the possibility to increase the capacity of radio communication under certain

conditions [13]. Recently, the generation of OAM beams in microwave range has been reported in many works [14]–[16]. As a potential method to improve the spectrum efficiency, OAM beam has become a hot research spot in microwave field [17]–[19].

Since the first simulation proposed by Thidé [20], various methods have been developed to generate OAM radio beams [21], such as spiral phase plates [22], [23], spiral reflectors [24], metasurface [25] and antenna arrays [26]–[28]. Although the first three methods can successfully transform a plane wave into an OAM radio wave through transmission or reflection, the inherent complex processing and single operating frequency restrict their further development. The antenna array, conformed circular distribution, generally needs a feed network or other devices to provide appropriate signals for each element. To generate an OAM beam, these signals are required to get the same amplitude and suitable phase shift. The specific phase shift between adjacent antennas depends on the mode of the OAM beam and the number of antennas in the antenna array. As a consequence, the antenna systems in generating OAM beams are too complex to meet these conditions.

To simplify the OAM antenna array, a system formed by global positioning system (GPS) ceramic antennas that avoids the use of phase shifting devices is proposed. The distinct advantages of GPS ceramic antenna such as circular polarization, high precision, low profile, etc. can make this antenna system perform better. In particular, the combination of circular polarization and circular distribution is the key point to realize the automatic phase modification. The utilization of power divider and coaxial line connecting make the proposed system simple and flexible. Furthermore, the problem of divergence angle of OAM beam can also be greatly improved by such a simplified antenna array system.

Section 2 presents the design of GPS ceramic antenna and its polarized characterization. Section 3 describes the simulations and measurements of generating OAM beams by the GPS ceramic antenna array. Finally, in Section 4, we draw the conclusions.

2. GPS Ceramic Antenna: Design and Characterization

To date, cut corner rectangle is a simple structure that is widely used in the design of circular polarization (CP) antenna [29], [30]. Its side length determines the resonant frequency of CP antenna. Cutting corner and center offset of feed point aim to achieve the CP of antenna. Here, the resonant frequency of the antenna is determined to be 1.550 GHz to meet the application of GPS. By means of calculation and optimization, the side length of radiation patch and cut corner are set to be 19 mm and 1.3 mm, respectively. The proposed antenna is designed on a ceramic substrate with a thickess of 4 mm and the relative permittivity of 21.4. And the radius of the chamfer is set to 4 mm to protect the antenna. Only in *y* direction, the center offset gets a non-zero value of 1.1 mm. The radiation patch, chamfered rectangular ceramic dielectric layer and ground plane together compose the GPS ceramic antenna.

Numerical predictions of the reflection coefficients for the GPS ceramic antenna were made using the commercial time-domain package CST Microwave Studio TM. Fig. 1 shows the measured and simulated results. The inserted illustration is the configuration of the GPS ceramic antenna. In the simulation, all boundaries are set as open (add space), and the direction of propagation is along *z*-axis. In the experimental setup, the proposed antenna is operated at 1.550 GHz frequency, which is applicable for GPS. From Fig. 1, it can be seen that the measured result coincides well with the simulated one, which demonstrates the reasonableness of the proposed design. Fig. 2(a) shows the axial ratio of the proposed antenna from 1.540 to 1.560 GHz. At its resonant frequency of 1.550 GHz, the axial ratio is less than 3 dB. Therefore, this antenna can be regarded as a CP antenna. In Fig. 2(b), the nearly circular radiation pattern of the GPS ceramic antenna in *x*-*y* plane at the resonant frequency of 1.550 GHz well illustrates the omnidirectional properties of the proposed antenna.

Fig. 3(a) and (b) show the measured and simulated radiation patterns at 1.550 GHz in *x*-*z* and *y*-*z* planes, respectively. It is seen that the measured results are basicly in good agreement with

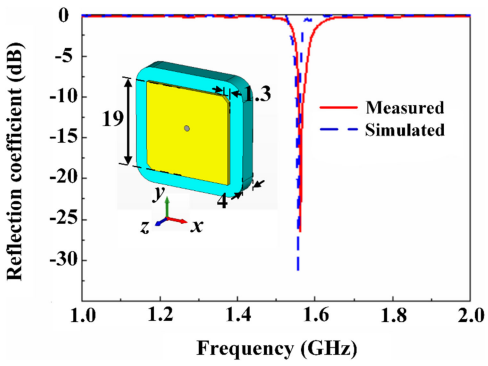

Fig. 1. Measured and simulated reflection coefficients of the GPS ceramic antenna.

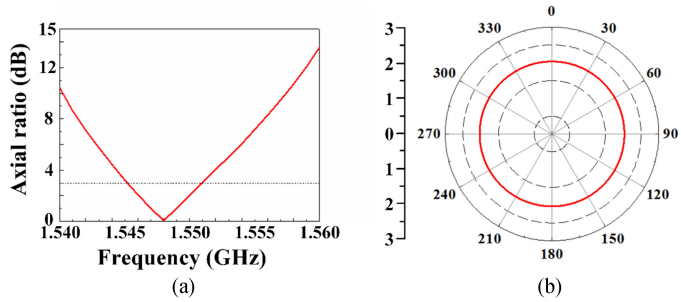

Fig. 2. Simulated axial ratio of the GPS ceramic antenna. (b) Simulated radiation pattern of the GPS ceramic antenna at 1.550 GHz in *x-y* plane.

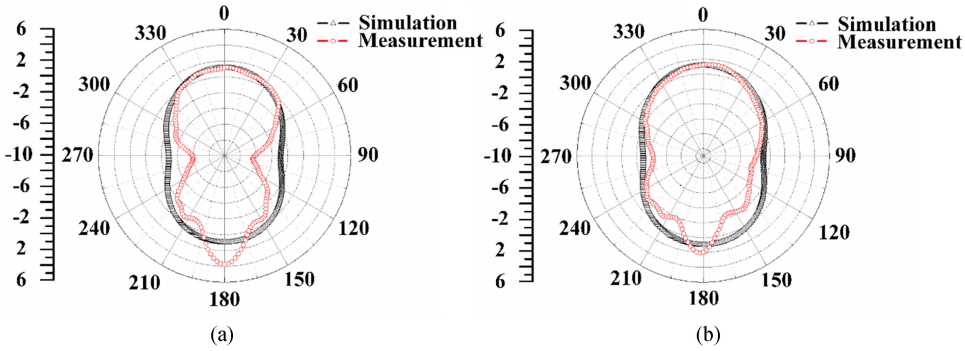

Fig. 3. Measured and simulated radiation patterns at 1.550 GHz in (a) *x-z* plane and (b) *y-z* plane.

the simulation results, although there is a discrepancy in the back lobes. This discrepancy is mainly caused by the support frame and feeder.

In the design of the CP antenna, adopting the cut corner rectangle structure as radiation patch can help to realize the conversion between right hand (RH) CP and left hand (LH) CP. The conversion of the two states can be realized by simply changing the direction of cut corner. As shown in Fig. 4, the electric field vectors for the antennas with different cut corner directions in one period obey the right hand rule and left hand rule, respectively. For the RHCP antenna, the Electric field vectors rotate counterclockwise a circle when the phase changes from 0° to 270°. In the case of LHCP antenna, there is a clockwise rotation, which means the transformation of CP state. The two CP states are then used to generate the plus-and-negative mode OAM beams.

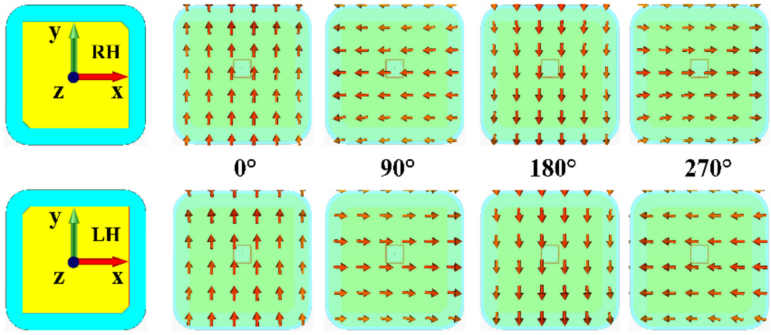

Fig. 4. Electric field vectors for RHCP and LHCP in one period at 1.550 GHz.

3. Results Antenna Array: Generation of OAM Beam

Traditionally, to generate the OAM beam with mode of $\pm l$, antennas are fed with signals of the same amplitude but different phases. The phase of the feeding signals is increased, in a turn, by $\pm 2\pi l$, where l is the mode of OAM beam. According to Nyquist theorem, a proper number of antennas needs to be greater than $2|l| + 1$ [20]. Generation of OAM beams by CP antenna array are firstly reported in [31]. These OAM radio beams are considered as the combination of two orthogonal line polarizations with 90° phase shifts. However, the complex structure is an obvious disadvantage of the CP antennas. And the application of the feed network makes the antenna array can operate only at a single frequency, thus limiting its flexibility. In our work, a GPS ceramic antenna array is used to generate OAM beams with the mode of ± 1 at the resonant frequency of 1.550 GHz. The minimum number of elements of the array is 4. However, the antenna number usually increases for standard waveform of the OAM beams. Therefore, six GPS ceramic antennas are suitable. It is worth noting that the antenna orientations are different with conventional ones. In the conventional method, the orientations of all antennas are the same [19], [27]. While the antennas in our system point to the center of the array. That is to say, the antennas are rotationally symmetric refer to the center. In this way, the antenna array can generate OAM beam by signals with the same amplitude and phase.

Fig. 5 shows the configuration of the antenna array and the simulation results. The RHCP antenna array shown in Fig. 5(a) consists of six RHCP GPS ceramic antennas evenly distributed on the circumference of a circle with $0.5\lambda_0$ radius. Simulation results of radiation pattern shown in Fig. 5(b) and phase distribution shown in Fig. 5(c) demonstrate that a standard OAM beam with mode of -1 is generated. Fig. 5(d), (e) and (f) illustrate the generation of OAM beam with mode of 1 when the antenna array consists of six LHCP GPS ceramic antennas. In addition, the polarization characteristic of GPS antenna is a benefit for OAM beam to reduce the divergence angle according to the radiation patterns.

We can find from Fig. 5(b) and (e) that there is no sidelobe and small divergence angle in the radiation pattern of OAM beam with ± 1, which mainly benefits from the small distribution radius of the antenna array and omnidirectional properties of the CP antenna. These simulation results confirm the well performances of the GPS ceramic antenna array in generating OAM beams. It is worth mentioning that the axial ratio of the generated OAM is 19.8 dB. According to the successful experience of generating OAM beam with $l = \pm 1$, it is not hard to form beams with a large mode using the proposed method. We only need to change the phase difference $\Delta\varphi$ of adjacent antenna to $l{\cdot}\Delta\varphi$, where $\Delta\varphi = 2\pi/N$ (N is the antenna number of the array). For example, the antenna array used to the generate OAM beam with $l = 2$ is shown in Fig. 5(g). The array includes 1 RHCP antennas. Therefore, phase difference of adjacent antenna is set to 60°. The radiation pattern and phase distribution of the generated OAM beam are illustrated in Fig. 5(h) and (i), respectively.

Ulteriorly, an OAM beam measurement system is designed to detect the actual effect of OAM beam that generated by an array involving the GPS ceramic antenna. In this system, six GPS

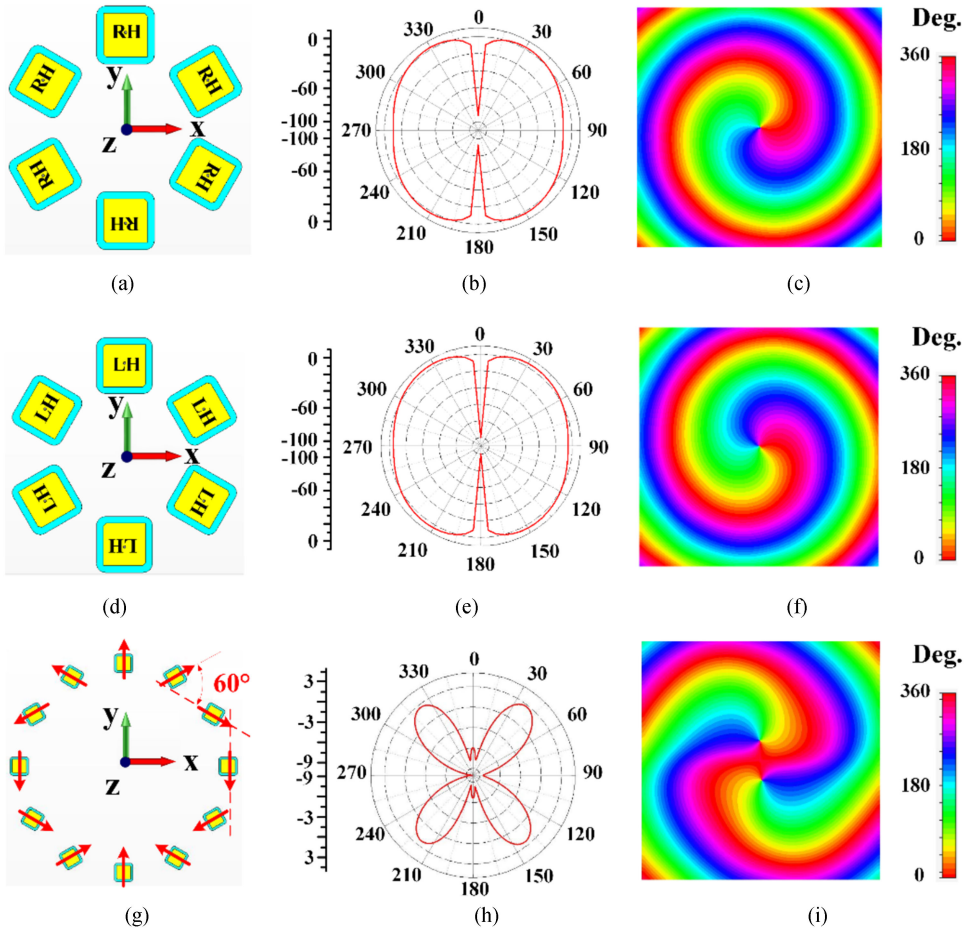

Fig. 5. Simulation of RHCP antenna array and LHCP antenna array at the resonant frequency of 1.550 GHz. (a) Configuration of RHCP antenna array. (b) Radiation pattern of RHCP antenna array in y-z plane with. (c) Phase distribution of RHCP antenna array. (d) Configuration of LHCP antenna array. (e) Radiation pattern of LHCP antenna array in y-z plane. (f) Phase distribution of LHCP antenna array. (g) Configuration of RHCP antenna array with 12 antennas. (h) Radiation pattern of OAM beam with $l = 2$. (i) Phase distribution of OAM beam with $l = 2$.

ceramic antennas with RHCP form the antenna array. It is similar in the case of LHCP. In the choice of the antenna number for the array, as odd will cause deformation of the OAM beam, the number of antenna need to be even. And the radius of antenna array r is $0.5\lambda_0$ to keep the array side lobes at low level and give enough space for each antenna. Six antennas are evenly distributed on the circumference. Thus, the angle θ between each antenna is 60°. The setup of the measurement system is shown in Fig. 6(a) and (b). A signal with the frequency of 1.550 GHz came from port 1 of vector network analyzer (VNA) is equally divided into six signals after passing a power divider. These signals are directly utilized to feed the antenna array with the help of coaxial lines. Then, the power and phase of the OAM beam with mode of -1 are detected by the receiving antenna with the help of liner guide rail. The center points of the guide rail and antenna array are both at *z*-axis, and the guide rail is parallel to the antenna array (*x*-*y* plane). Finally, the detected signal is transmitted back to port 2 of the VNA. To test the electromagnetic performance of the antenna array, the reflection coefficient is measured and the results are shown in Fig. 6(c). The agreement between Fig. 6(c) and Fig. 1 verifies the normal operation of the proposed antenna in the array and system.

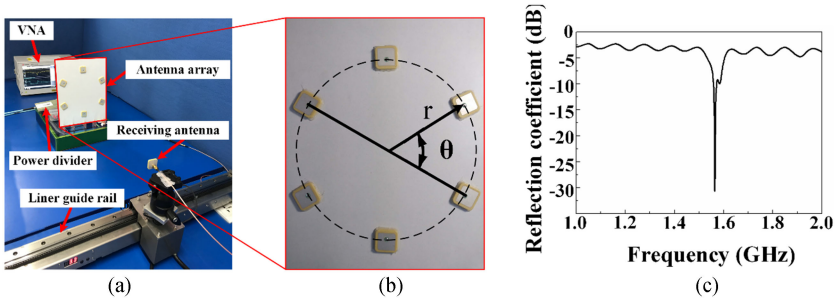

Fig. 6. Measurement system for generation of OAM beam. (b) Details of the antenna array. (c) The measured reflection coefficient of the proposed antenna array.

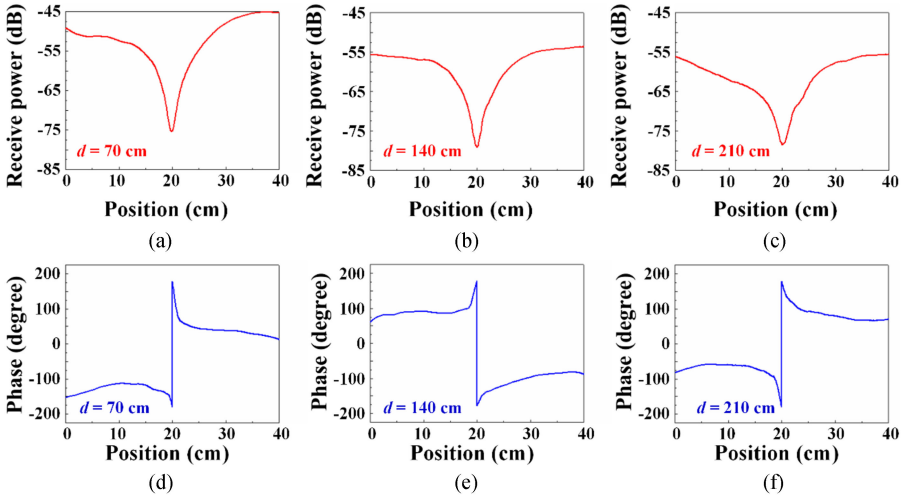

Fig. 7. Observed receiving power and phase distribution of the generated OAM beam at various distances away from the antenna array: (a) receiving power at 70 cm; (b) receiving power at 140 cm; (c) receiving power at 210 cm; (d) phase distribution at 70 cm; (e) phase distribution at 140 cm; (f) phase distribution at 210 cm.

As mentioned above, a receiving antenna and a liner guide rail are used to detect the one-dimensional spatial distribution of the OAM beam's electromagnetic characteristic at various distances away from the antenna array. The observed results are depicted in Fig. 7, which includes a range from 0 to 40 cm. The sharp center decrease of the receiving powers and the 360° phase mutation in Fig. 7 are obvious characteristics of OAM beam, which can be easily found in Fig. 5. As shown in Fig. 5, the sharp decrease and mutation emerge when the receiving antenna passes through the phase singularity. Because in this setup, the division of power and the long-distance transmission in cables cause enormous loss, the received powers shown in Fig. 7 are low. However, by comparing Fig. 7(a), (b) and (c), it can be found that the receive power only reduces a bit with the increase of the detection distance. Although the output power of VNA is only 0 dBm, the detectable distance can reach 210 cm.

The proposed GPS ceramic antenna array size, complexity and detection range are compared with some recent publications in Table 1. In this work, the radius of the distribution can reach the minimum value of 0.5λ0. With no phase shifting device, the proposed GPS ceramic antenna array can greatly simplify the OAM generation system. The characteristics of the OAM shown in Fig. 7 is very obvious. Moreover, the measurement range up to 2.1 m has been demonstrated in this paper. According to Table 1, the proposed antenna array obtains well performances in terms of size, complexity and detection range.

TABLE 1
Comparison Between Proposed and Reported OAM Antenna Array

Ref.	Radius of distribution	Phase shifting device
[31]	$0.7\lambda_0$	feeding network
[32]	$4.2\lambda_0$	delayed signals
[33]	$0.9\lambda_0$	rotman lenses
[34]	$2.0\lambda_0$	optical spectrum processor
[35]	$0.8\lambda_0$	different length cables
[36]	$5.0\lambda_0$	phase shifters
[37]	$3.0\lambda_0$	different length cables
[38]	$1.0\lambda_0$	feeding network
[39]	$0.6\lambda_0$	feeding network
[40]	$1.6\lambda_0$	feeding network
This work	$0.5\lambda_0$	none

4. Conclusions

A GPS ceramic antenna is designed and applied to generate OAM beam in radio domain. By changing the direction of the cut corner on the rectangle radiation patch, the CP state can be altered. A significantly simplified GPS ceramic antenna array with RHCP state is used to generate the OAM beam with negative mode. Similarly, GPS ceramic antenna array with LHCP state can generate the OAM beam with plus mode. By simulating the GPS ceramic antenna arrays, two kinds of OAM beams with standard spiral shape are successfully obtained. In particular, the radiation pattern of the OAM beam generated by the GPS ceramic antenna array shows quite small divergence angle and no side lobe, which confirms the excellent property of the antenna array in launching standard OAM beams. A series of experiments are designed and performed to test the electromagnetic characteristic of the OAM beams at different distances away from the antenna array. The OAM beams located at more than 2 meters away from the antenna array still can be detected when the output signal power is 0 dBm. After comparing with some recent publications, this approach is believed to be a great progress in the generation of high-quality OAM beam.

References

[1] M. Padgett and L. Allen, "Light with a twist in its tail," *Contemporary Phys.*, vol. 41, no. 5, pp. 275–285, 2000.
[2] J. Leach, M. J. Padgett, S. M. Barnett, S. Franke-Arnold, and J. Courtial, "Measuring the orbital angular momentum of a single photon," *Phys. Rev. Lett.*, vol. 88, no. 1, 2002, Art. no. 257901.
[3] J. Xu *et al.*, "A wideband F-shaped microstrip antenna," *IEEE Antennas Wireless Propag. Lett.*, vol. 16, pp. 829–832, 2016.
[4] D. Mcgloin, N. B. Simpson, and M. J. Padgett, "Transfer of orbital angular momentum from a stressed fiber-optic waveguide to a light beam," *Appl. Opt.*, vol. 37, no. 3, pp. 469–472, 1998.
[5] M. Padgett and R. Bowman, "Tweezers with a twist," *Nature Photon.*, vol. 5, no. 6, pp. 343–348, 2011.
[6] T. Yuan, H. Wang, Y. Qin, and Y. Cheng, "Electromagnetic vortex imaging using uniform concentric circular arrays," *IEEE Antennas Wireless Propag. Lett.*, vol. 15, pp. 1024–1027, 2016.
[7] L. Torner, J. P. Torres, and S. Carrasco, "Digital spiral imaging," *Opt. Exp.*, vol. 13, no. 3, pp. 873–81, 2005.
[8] L. Paterson, M. P. Macdonald, J. Arlt , W. Sibbett, P. E. Bryant, and K. Dholakia, "Controlled rotation of optically trapped microscopic particles," *Science*, vol. 292, no. 5518, pp. 912–914, 2001.
[9] D. G. Grier, "A revolution in optical manipulation," *Nature*, vol. 424, no. 6950, pp. 810–816, 2003.
[10] H. Xu *et al.*, "Switchable complementary diamond-ring-shaped metasurface for radome application," *IEEE Antennas Wireless Propag. Lett.*, vol. 17, no. 12, pp. 2494–2497, 2018.
[11] K. Bi *et al.*, "Ultrafine core-shell $BaTiO_3$@SiO_2 structures for nanocomposite capacitors with high energy density of ferrite rods and metallic slits," *Nano Energy*, vol. 51, pp. 513–523, 2018.
[12] J. Wang *et al.*, "Terabit free-space data transmission employing orbital angular momentum multiplexing," *Nature Photon.*, vol. 6, no. 7, pp. 488–496, 2012.
[13] F. Tamburini, E. Mari, A. Sponselli, B. Thidé, A. Bianchini, and F. Romanato, "Encoding many channels in the same frequency through radio vorticity: First experimental test," *New J. Phys.*, vol. 14, no. 3, pp. 811–815, 2011.
[14] X. T. Wang, Y. Cui, T. Li, M. Lei, J. Li, and Z. Wei, "Recent advances in the functional 2D photonic and optoelectronic devices," *Adv. Opt. Mater.*, vol. 7, no. 3, 2019, Art. no. 1801274. DOI: 10.1002/adom.201801274.

[15] S. Yu, L. Li, G. Shi, C. Zhu, X. Zhou, and Y. Shi, "Design, fabrication, and measurement of reflective metasurface for orbital angular momentum vortex wave in radio frequency domain," *Appl. Phys. Lett.*, vol. 108, 2016, Art. no. 121903.
[16] S. Lin *et al.*, "Roll-to-roll production of transparent silver nanofiber network electrode for flexible electrochromic smart windows," *Adv. Mater.*, vol. 29, 2017, Art. no. 1703238.
[17] N. Bozinovic *et al.*, "Terabit-scale orbital angular momentum mode division multiplexing in fibers," *Science*, vol. 340, no. 6140, p. 1545–1548, 2013.
[18] K. Bi, W. T. Zhu, M. Lei, and J. Zhou, "Magnetically tunable wideband microwave filter using ferrite-based metamaterials," *Appl. Phys. Lett.*, vol. 106, 2015, Art. no. 173507.
[19] Q. Wang, X. Li, L. Y. Wu, P. F. Lu, and Z. F. Di, "Electronic and interface properties in graphene oxide/hydrogen-passivated ge heterostructure," *Phys. Status Solidi RRL*, vol. 13, 2019, Art. no. 1800461. DOI: 10.1002/pssr.201800461.
[20] B. Thidé *et al.*, "Utilization of photon orbital angular momentum in the low-frequency radio domain," *Phys. Rev. Lett.*, vol. 99, no. 8, 2007, Art. no. 087701.
[21] A. Tennant and B. Allen, "Generation of OAM radio waves using circular time-switched array antenna," *Electron. Lett.*, vol. 48, no. 21, pp. 1365–1366, 2012.
[22] P. Schemmel, G. Pisano, and B. Maffei, "Modular spiral phase plate design for orbital angular momentum generation at millimetre wavelengths," *Opt. Exp.*, vol. 22, no. 12, 2014, Art. no. 14712.
[23] X. Hui *et al.*, "Ultralow reflectivity spiral phase plate for generation of millimeter-wave OAM Beam," *IEEE Antennas Wireless Propag. Lett.*, vol. 14, pp. 966–969, 2015.
[24] F. Tamburini, E. Mari, B. Thindé, C. Barbieri, and F. Romanato, "Experimental verification of photon angular momentum and vorticity with radio techniques," *Appl. Phys. Lett.*, vol. 99, no. 20, p. 321, 2011, Art. no. 204102.
[25] L. Cheng, W. Hong, and Z. C. Hao, "Generation of electromagnetic waves with arbitrary orbital angular momentum modes," *Sci. Rep.*, vol. 4, 2014, Art. no. 4814.
[26] Q. Bai, A. Tennant, and B. Allen, "Experimental circular phased array for generating OAM radio beams," *Electron. Lett.*, vol. 50, no. 20, pp. 1414–1415, 2014.
[27] X. Gao *et al.*, "An orbital angular momentum radio communication system optimized by intensity controlled masks effectively: Theoretical design and experimental verification," *Appl. Phys. Lett.*, vol. 105, 2014, Art. no. 241109.
[28] L. Y. Wu *et al.*, "Stanene nanomeshes as anode materials for Na-ion batteries," *J. Mater. Chem. A*, vol. 6, pp. 7933–7941, 2018.
[29] O. P. Falade, M. U. Rehman, Y. Gao, X. Chen, and C. G. Parini, "Single feed stacked patch circular polarized antenna for triple band GPS receivers," *IEEE Trans. Antennas Propag.*, vol. 60, no. 10, pp. 4479–4484, Oct. 2012.
[30] Y. Huang, L. Yang, J. Li, and G. Wen, "Polarization conversion of metasurface for the application of wide band low-profile circular polarization slot antenna," *Appl. Phys. Lett.*, vol. 109, no. 5, 2016, Art. no. 054101.
[31] F. Spinello *et al.*, "Experimental near field OAM-based communication with circular patch array," 2015. arXiv:1507.06889.
[32] X. D. Bai *et al.*, "Experimental array for generating dual circularly-polarized dual-mode OAM radio beams," *Sci. Rep.*, vol. 7, 2017, Art. no. 40099.
[33] G. Xie *et al.*, "Demonstration of tunable steering and multiplexing of two 28 GHz data carrying orbital angular momentum beams using antenna array," *Sci. Rep.*, vol. 6, 2016, Art. no. 37078.
[34] C. Xu *et al.*, "Free-space radio communication employing OAM multiplexing based on rotman lens," *IEEE Microw. Wireless Compon. Lett.*, vol. 26, no. 9, pp. 738–740, Sep. 2016.
[35] G. Xinlu *et al.*, "Generating the orbital angular momentum of radio frequency signals using optical-true-time-delay unit based on optical spectrum processor," *Opt. Lett.*, vol. 39, no. 9, pp. 2652–2655, 2014.
[36] K. Liu *et al.*, "Generation of OAM beams using phased array in the microwave band," *IEEE Trans Antennas Propag.*, vol. 64, no. 9, pp. 3850–3857, Sep. 2016.
[37] Y. Gong *et al.*, "Generation and transmission of OAM-carrying vortex beams using circular antenna array," *IEEE Trans Antennas Propag.*, vol. 65, no. 6, pp. 2940–2949, Jun. 2017.
[38] H. Yao *et al.*, "Patch antenna array for the generation of millimeter-wave Hermite-Gaussian beams," *IEEE Antennas Wireless Propag. Lett.*, vol. 15, pp. 1947–1950, 2016.
[39] B. Y. Liu, Y. H. Cui, and R. Li, "A broadband dual-polarized dual-OAM-Mode antenna array for OAM communication," *IEEE Antennas Wireless Propag. Lett.*, vol. 16, pp. 744–747, 2017.
[40] Z. G. Guo and G. M. Yang, "Radial uniform circular antenna array for dual-mode OAM communication," *IEEE Antennas Wireless Propag. Lett.*, vol. 16, pp. 404–407, 2017.